THE JOURNAL OF BIOLOGICAL CHEMISTRY VOL. 285, NO. 17, pp. 12873–12881, April 23, 2010


# The Structure of Mammalian Serine Racemase

## *EVIDENCE FOR CONFORMATIONAL CHANGES UPON INHIBITOR BINDING*[S]

Received for publication, August 7, 2009, and in revised form, January 5, 2010 Published, JBC Papers in Press, January 27, 2010, DOI 10.1074/jbc.M109.050062

**Myron A. Smith**[1], **Volker Mack, Andreas Ebneth, Isabel Moraes, Brunella Felicetti, Michael Wood, Dorian Schonfeld, Owen Mather, Andrea Cesura, and John Barker**

*From the Department of Structural Biology and Biology, Evotec, 114 Milton Park, Abingdon, Oxon OX14 4SA, United Kingdom*

**Serine racemase is responsible for the synthesis of D-serine, an endogenous co-agonist for *N*-methyl-D-aspartate receptor-type glutamate receptors (NMDARs). This pyridoxal 5′-phosphate-dependent enzyme is involved both in the reversible conversion of L- to D-serine and serine catabolism by *α*,*β*-elimination of water, thereby regulating D-serine levels. Because D-serine affects NMDAR signaling throughout the brain, serine racemase is a promising target for the treatment of disorders related to NMDAR dysfunction. To provide a molecular basis for rational drug design the x-ray crystal structures of human and rat serine racemase were determined at 1.5- and 2.1-Å resolution, respectively, and in the presence and absence of the orthosteric inhibitor malonate. The structures revealed a fold typical of *β*-family pyridoxal 5′-phosphate enzymes, with both a large domain and a flexible small domain associated into a symmetric dimer, and indicated a ligand-induced rearrangement of the small domain that organizes the active site for specific turnover of the substrate.**

*N*-Methyl-D-aspartate receptor-type glutamate receptors (NMDARs)[2] are a key component in glutamatergic transmission implicated in the development, function, and plasticity of the nervous system. In addition to the neurotransmitter glutamate, the activation of NMDARs requires the binding of either of the two endogenous co-agonists, glycine or D-serine, to the NMDAR "glycine modulatory site" (1, 2). Although both amino acids have similar potency as co-agonists, they display regional differences in modulating NMDAR function (3, 4). According to its distribution within the CNS, D-serine exerts its function predominantly in corticolimbic brain structures (5). This pivotal role of D-serine is supported by several experimental findings, including depletion studies in neuronal tissue preparations, indicating a strong reduction in NMDAR-mediated transmission and impaired synaptic plasticity in the absence of D-serine (6, 7).

D-serine is produced by enzymatic conversion of L- to D-serine mediated by the pyridoxal 5′-phosphate (PLP)-containing enzyme serine racemase (SR). Mammalian SR was first purified from rat brain and functionally characterized in 1999 by Wolosker and colleagues (8). The enzyme is expressed in glial cells and neurons and constitutes the sole endogenous source for D-serine in mammals (9). Both human and rodent SR have been purified and extensively studied to generate comprehensive knowledge of the enzymatic characteristics and allosteric modulation by a number of agents such as ATP and $Mg^{2+}$ ions.

In addition to serine isomerization, the enzyme catalyzes the *α*,*β*-elimination of water from L- and D-serine to produce pyruvate and ammonia, thus, offering the possibility for SR not only to elevate but also to reduce the level of D-serine (5), a role that previously has mainly been attributed to D-amino acid oxidase (10).

Recent data from SR-deficient mice strongly implicate this enzyme in the process of NMDAR-dependent plasticity and neurotoxicity. Knock-out mice were shown to have severely reduced D-serine levels with the consequence of impaired NMDAR-mediated transmission, long term potentiation, and attenuated NMDA- and A*β*1–42-induced toxicity in the hippocampus and cerebral cortex (5, 11). These results emphasize the importance of SR as a pharmacological target to treat neuropathological conditions associated with dysfunction in NMDAR neurotransmission. Overactivation of NMDARs is involved in acute and progressive neurodegenerative diseases such as stroke, amyotrophic lateral sclerosis, and Huntington, Alzheimer, and Parkinson diseases (12). In addition, considerable evidence was found for enhanced NMDAR-mediated transmission and plasticity as a potential cause for pain conditions, *e.g.* neuropathic pain (13).

Pharmacological intervention with SR activity constitutes an innovative strategy to treat neurological disorders. To pave the way for rational drug design by means of fragment-based screening and related *in silico* approaches we wished to determine the x-ray crystal structure of mammalian SR. In this study we provide the first crystal structures of mammalian SR both as a holoenzyme and complexed with an inhibitor. This information will be important for the rational design of novel drugs for the treatment of diverse neurological diseases.

## EXPERIMENTAL PROCEDURES

*Human and Rat SR Cloning, Expression, and Purification*—Two point mutations (C2D and C6D) were introduced by site-directed mutagenesis (QuikChange II, Stratagene) into a wild-

*The atomic coordinates and structure factors (codes 3L6B, 3L6R, 3L6C, and 3HMK) have been deposited in the Protein Data Bank, Research Collaboratory for Structural Bioinformatics, Rutgers University, New Brunswick, NJ (http://www.rcsb.org/).*

[S] The on-line version of this article (available at http://www.jbc.org) contains additional crystallographic data figures.

[1] To whom correspondence should be addressed. Tel.: 44-1235-838-864; Fax: 44-1235-838-931; E-mail: myron.smith@evotec.com.

[2] The abbreviations used are: NMDAR, *N*-methyl-D-aspartate receptor-type glutamate receptor; PLP, pyridoxal 5′-phosphate; SR, serine racemase; hSR, human serine racemase; rSR, rat serine racemase; SDH, serine dehydratase; CHES, 2-(cyclohexylamino)ethanesulfonic acid; Bis-Tris, 2-[bis(2-hydroxyethyl)amino]-2-(hydroxymethyl)propane-1,3-diol; r.m.s.d., root mean square deviation.

type pET24a construct. After DNA sequence verification, plasmid DNA was transformed into *Escherichia coli* Rosetta 2 (DE3) cells for expression at 37 °C in 9 liters of 2×YT medium (16 g of Tryptone, 10 g of yeast extract, and 5 g of NaCl in 1 liter of $H_2O$) supplemented with 50 μg/ml kanamycin and 0.01% pyridoxine. The cells were grown to an optical density at 600 nm of 0.6., at which point isopropyl 1-thio-β-D-galactopyranoside was added to a final concentration of 0.5 mM, and the cells were incubated for a further 16 h at 25 °C. The cells were harvested by centrifugation at 5,000 × *g* for 10 min and stored at −80 °C. Next the cell pellet was lysed by sonication and centrifuged for 60 min at 4 °C at 16,500 rpm. All the purification steps were performed at 4 °C. Because all the proteins had been expressed with a histidine tag purification of each protein was initially performed by affinity chromatography with a Talon column. The fractions were analyzed by SDS-PAGE, and the protein-containing samples were collected and loaded onto a Superdex 200 (16/60) column equilibrated with 20 mM Tris-HCl, pH 8.0, 100 mM NaCl, 10% glycerol, 50 μM PLP, 2 mM $MgCl_2$, 5 mM dithiothreitol. The fractions that contained >98% pure SR, after SDS-PAGE analysis, were collected, pooled, concentrated to 10 mg/ml, flash frozen in liquid nitrogen, and stored at −80 °C. Selenomethionine-labeled protein was expressed using B834(DE3) cells (Novagen), and purification followed the same protocol as human SR mutant.

*Oligomeric Analysis of Recombinant SR*—A Superdex 200 5/150 column was calibrated with proteins, including Dextran blue (2000 kDa), aldolase (156.8 kDa), conalbumin (75 kDa), ovalbumin (43 kDa), carbonic anhydrase (29 kDa), and ribonuclease A (13.7 kDa). Aliquots of each enzyme (50 μl at 10 mg/ml) were loaded onto the column and equilibrated with 20 mM Tris-HCl, pH 8.0, 100 mM NaCl, 10% glycerol, 50 μM PLP, 2 mM $MgCl_2$, 5 mM dithiothreitol. The flow rate was kept at 0.3 mg/ml. The elution volume of each molecular weight standard was recorded, and a calibration curve was obtained by plotting the elution volume of the protein (milliliters) against the log of the molecular mass. An aliquot of human SR (hSR) mutant with Cys-2 and Cys-6 mutated to Asp (hSR_C2,6D_CHis, 50 μl at 2 mg/ml) was also loaded onto the same column under the same conditions, and the elution volume was recorded. Dynamic light scattering experiments were performed with a Viscotek 802 system on SR samples of 1 and 5 mg/ml concentration in 20 mM Tris, pH 8.0, 100 mM NaCl, 10% glycerol, 50 μM PLP, 1 mM $MgCl_2$, 5 mM dithiothreitol at 22 °C.

Cross-linking experiments with hSR_C2,6D_CHis. Aliquots of hSR_C2,6D_CHis (20 μl, 10 mg/ml in buffer B) were diluted 1:10 with phosphate-buffered saline buffer, pH 7.4. Each aliquot was incubated with different concentrations of glutaraldehyde ranging from 0.0005% to 1%. Each sample was incubated for 5 min at 37 °C. The reactions were stopped by adding 2 μl of 1 M Tris-HCl, pH 8.0.

*Enzyme Assay*—To determine the activity of purified SR, a fluorometric assay was used with L-serine as a substrate, coupling the formation of D-serine to D-amino acid oxidase and horseradish peroxidase (Sigma-Aldrich), plus the peroxidase substrate AmpLite (10-acetyl-3,7-dihydroxyphenoxazine, Bioquest). The D-serine produced during the incubation period was degraded by D-amino acid oxidase, generating keto acid, ammonia, and hydrogen peroxide. The generated hydrogen peroxide was quantified by addition of AmpLite, which reacts in a 1:1 stoichiometry with hydrogen peroxide in the presence of horseradish peroxidase to produce the highly fluorescent oxidation product, resorufin.

The activity of 100 nM purified SR was determined in 100 mM CHES (pH 9) containing 1 mM $MgCl_2$, 1 mM ATP, 10 μM PLP, 0,05% Pluronic F-127, and 0.5% bovine serum albumin. For D-serine detection 1.5 units/ml D-amino acid oxidase and 0.25 unit/ml horseradish peroxidase were added. The reactions were incubated at 37 °C, and fluorescence emission of resorufin was measured at 585 nm in a Tecan Saphire device. The D-serine concentration present in a given sample was determined by correlating the fluorescence with D-serine calibration curves.

*Crystallization and Data Collection*—The hSR double mutant concentrated to 10 mg/ml was crystallized by sitting drop, vapor diffusion with 25% polyethylene glycol 3350, 200 mM sodium malonate, and 50 mM $MnCl_2$ as the reservoir solution. Crystals appeared overnight and grew to 70 μm within 4 days. The crystal used for the diffraction experiment was cryoprotected by reservoir solution to which glycerol was added to make 20% v/v concentration cryoprotection solution. X-ray data were collected at the Diamond Light Source using the Area Detector Systems Corp. (ADSC) Quantum 315 charge-coupled device detector in beamline I04.

The selenomethionine-labeled hSR crystals grew under similar conditions and cryoprotection was also with 20% glycerol. X-ray data were collected at Diamond Light Source on beamline I04.

Rat SR (rSR) double mutant concentrated to 35 mg/ml was crystallized in 55% v/v Tacsimate (1.8305 M malonic acid, 0.25 M ammonium citrate tribasic, 0.12 M succinic acid, 0.3 M DL-malic acid, 0.4 M sodium acetate trihydrate, 0.5 M sodium formate, and 0.16 M ammonium tartrate dibasic), pH 8.0, 100 mM Bis-Tris propane, pH 7.8. Crystals grew to 50 μm after 10 days. The crystal used for the diffraction experiment was cryoprotected by reservoir solution to which 20% glycerol was added. X-ray data of the rSR malonate complex were collected in-house on a Rigaku RUH3R generator and an RAXIS IV++ image plate detector, and the rSR holoenzyme was collected at Diamond Light Source.

*Structure Determination*—The diffraction images of the hSR selenomethionine crystal were integrated and scaled using d*trek, and the selenium atoms were located using SHELX (14). After solvent flattening with SOLOMON (15) initial inspection of the maps revealed excellent density for the protein side chains, and the covalently linked PLP molecule was also easily visible. 95% of the structure was built using ARP/WARP (16), and the final model building was done manually with iterative refinement using REFMAC5 (17).

The diffraction images of hSR were integrated using MOSFLM (18) and scaled and truncated using SCALA (19, 20). The structure was determined using PHASER (21) molecular replacement software, and a model of human serine racemase was previously determined by selenomethionine single anomalous diffraction (Table 1). rSR integration and scaling were performed with D*TREK (22), and the structure was solved with PHASER (21) using the refined human SR model.

*Refinement*—After iterative cycles of rebuilding and refinement with REFMAC5 (17), the *R*-factor of hSR dropped 19.6%, while the free *R*-factor decreased 20.8%. TLS refinement was included toward the end using eight TLS groups and the final *R*-factor/$R_{free}$ was 16.7/17.7%. The stereochemistry was good with 92.1% of residues in the most favored region of the Ramachandran plot and 7.9% of residues in additionally allowed regions with none in the generously allowed or disallowed regions. The rSR refinement was performed with REFMAC5 after which the final *R*-factor/$R_{free}$ ratio was 22/26%. The stereochemistry was similar to human with 93% of residues in the most favored and 7% in the additionally allowed regions of the Ramachandran plot. Structure alignments were performed with COOT (23) and PyMOL (24).

## RESULTS

*Recombinant hSR and rSR*—Expression of wild-type SR in *E. coli* was found to yield very low levels of soluble protein. To overcome this issue a homology model of hSR (data not shown) based on the *Schizosaccharomyces pombe* SR structure (PDB code 1V71) was constructed. This model identified two N-terminal surface-exposed cysteines, Cys-2 and Cys-6, which were hypothesized to affect protein solubility. Indeed, mutation of these two cysteines into aspartic acids did improve protein expression and enabled the production of sufficient amounts of soluble enzyme. Biophysical and enzymatic activity characterization of the Cys-2 and Cys-6 mutant confirmed comparable properties to wild-type SR. Further stabilization was achieved by fusion of a His tag to the C terminus of SR. The optimized expression construct yielded soluble, stable, highly pure (>98% as judged by SDS-PAGE analysis), and homogeneous protein. Both the human and rat mutants were expressed and purified following similar protocols.

For further characterization of the quaternary protein structure we subjected the purified SR to size-exclusion chromatography. Upon gel-filtration chromatography on a Superdex 200 5/150 column (Amersham Biosciences), the purified SR preparation gave a clear symmetric peak corresponding to a theoretical mass of ~74 kDa, likely corresponding to the SR dimer. Subsequently, this observation was confirmed by cross-linking experiments with glutaraldehyde. The covalently linked dimer, visualized on SDS-PAGE, was the most abundant species, and formed at glutaraldehyde concentrations as low as 0.0005%. Dynamic light scattering experiments correlated well with the size-exclusion chromatography results with calculated masses for the hSR and rSR of ~75 kDa and a polydispersity index of 21%.

The activity of wild-type human and rat enzymes, as well as the corresponding C2DC6D-mutant forms was determined by a fluorometric assay based on the synthesis of D-serine and analyzed using Michaelis-Menten kinetics. All SR preparations were active and $K_m$ values obtained were in accordance with previously published data (8, 26, 27). Wild-type and mutant enzymes of the same species showed comparable $K_m$ values, whereas the $K_m$ for rSR (rSR, $K_m$ of 3.7 mM; rSR C2DC6D, $K_m$ of 4.5 mM) was slightly lower than for human SR (hSR, $K_m$ of 6.5 mM; hSR C2DC6D, $K_m$ of 7.7 mM). As previously reported, the activity of human and rat SR was strongly reduced by the competitive inhibitor malonate (28). Inhibition by malonate, determined at a substrate concentration of 5 mM L-serine, showed the predicted concentration-dependent behavior and revealed inhibition constants ($K_i$) of 59 and 111 $\mu$M on wild-type and mutant human SR, respectively, in agreement with previously published data (28). The affinity of malonate for rSR appeared substantially lower with a $K_i$ of 568 $\mu$M on the wild-type and 1599 $\mu$M on the mutant enzyme.

*Crystal Structure*—Human and rat holoenzymes were used for protein crystallization and yielded crystals diffracting to as high as 2.2 Å. Initially the *S. pombe* structure (PDB code 1V71) of serine racemase was used as the model for molecular replacement. Unfortunately, the density for a significant region spanning residues 70–155 of the human SR sequence, previously defined as the enzyme's small domain, was not interpretable. Further crystal screening was performed to improve crystal quality and to identify new crystal forms. Co-crystallizations with the substrate L-serine, glycine, the orthosteric inhibitor, malonate, and other small molecules were explored to determine if crystal quality could be improved. However, only malonate resulted in highly diffracting co-crystals. In addition, selenomethionine-labeled protein was produced to generate crystals for experimental phasing. After single anomalous diffraction data collection the structure was solved to 1.7 Å and was used as a model for subsequent structure solutions. The data collection and refinement statistics are shown in Table 1. Further optimization and screening experiments led to the crystallization of ligand-free rSR with significantly improved resolution of the small domain. The supplemental data show the electron density for human and rat SR contoured at 1$\sigma$, as well as the Ramachandran plots for each structure.

The structures of human and rat SR have an overall fold typical of $\beta$-family PLP-dependent enzymes. The secondary structure of the mammalian racemase is detailed in Fig. 1 highlighting the large and small domains. For simplicity all the numbering used throughout this discussion will correspond to the mammalian numbering, unless stated otherwise. The first 2 and last 17 residues of the hSR construct were not well defined in the electron density. In addition, the residues 69–73, those before the start of the small domain, were found to be disordered. These residues were not included in the final model.

PLP enzymes are categorized into five groups by similarity of their secondary structure. SR, as well as the closest homologue for which a crystal structure is available, serine dehydratase (SDH) (PDB codes 1PWH, 1PWE, and 1P5J) (29, 30), belong to the fold-type II group containing a large and small domain. Human SR and human SDH have 23% sequence identity and are structurally ~90% similar (Fig. 1). Both domains have the typical open $\alpha/\beta$ architecture characteristic of this family. The large PLP-containing domain has at its core a seven-stranded twisted $\beta$-sheet, with all but the first strand parallel, surrounded by ten helices. The small domain also has a twisted $\alpha/\beta$ architecture with four central parallel $\beta$-sheets, and three $\alpha$-helices arranged so that two (helices 4 and 5) are on one side of the sheet close to the domain interface, and one (helix 6) is on the other solvent-exposed side.

For SDH, the boundary between large and small domains is described differently with helix 3 included in the small

**TABLE 1**
**Crystallographic statistics of human and rat serine racemase**

| | Human selenomethionine | Human | Rat | Rat holo |
|---|---|---|---|---|
| **Data collection** | | | | |
| Space group | $P2_12_12$ | $P2_12_12$ | P3 | $P2_12_12_1$ |
| Cell dimensions | | | | |
| *a*, *b*, *c* (Å) | 54.54, 84.21, 70.38 | 54.57, 84.29, 69.98 | 110.59, 110.59, 47.92 | 48.26, 102.96, 120.92 |
| $\alpha,\beta,\gamma$ (°) | 90.00, 90.00, 90.00 | 90.00, 90.00, 90.00 | 90.00, 90.00, 120.00 | 90.00, 90.00, 90.00 |
| Resolution (Å) | 45.78 (1.70) | 38.3 (1.50) | 55.3 (1.95) | 47.4 (1.8) |
| $R_{sym}$ or $R_{merge}$ | 9.4 (28.1) | 4.9 (27.5) | 6.0 (31.1) | 6.9 (19.5) |
| $I/\sigma I$ | 16.1 (4.5) | 13.9 (4.4) | 9.4 (2.1) | 10.1 (3.5) |
| Completeness (%) | 97.1 (78.9) | 98.63 (99.97) | 95.9 (71.3) | 94.8 (74.8) |
| Redundancy | 12.45 (5.44) | 3.7 (3.7) | 2.5 (1.6) | 3.17 (1.95) |
| **Phasing** | | | | |
| Selenium atoms found by SHELX | 4 | | | |
| Mean FOM | 0.45 | | | |
| Mean FOM after DM | 0.65 | | | |
| **Refinement** | | | | |
| Resolution (Å) | 45.8-1.7 | 36.1-1.5 | 47.9-2.2 | 41.1-2.1 |
| No. reflections | 33,537 | 49,358 | 30,285 | 32,657 |
| $R_{work}/R_{free}$ | 16.8/20.2 | 16.7/17.7 | 21.6/26.7 | 24.1/28.9 |
| No. molecules in asu | 1 | 1 | 2 | 2 |
| No. atoms | | | | |
| Protein | 2,472 | 2,441 | 4,779 | 4,844 |
| Ligand/ion | 23 | 23 | 46 | 32 |
| Water | 305 | 244 | 80 | 202 |
| *B*-factors | | | | |
| Wilson *B*-factor | 18.8 | 15.9 | 38.2 | 23.8 |
| Protein | 21.2 | 8.8 | 47.8 | 29.6 |
| Ligand/ion | 15.7 | 10.0 | 36.6 | 19.7 |
| Water | 23.4 | 33.2 | 36.8 | 28.0 |
| r.m.s.d. | | | | |
| Bond lengths (Å) | 0.03 | 0.009 | 0.015 | 0.007 |
| Bond angles (°) | 2.0 | 1.2 | 1.6 | 1.0 |

domain. The SDH small domain, therefore, has four $\alpha$-helices and four $\beta$-sheets (29, 30). Importantly, helix 3 in the SR structure precedes a mobile hinge region (69–77) connecting the small and the large domains. This helix, as will be discussed later, is not involved in the rearrangement of the small domain. Based on our observations of the x-ray crystal structure of serine racemase we have included helix 3 (residues 55–67), containing the catalytic lysine (Lys-56), into the large domain (Fig. 1). Thus, the large PLP-containing domain of SR is constituted of residues 1–68 and 157–340, and the small domain spans residues 78–155 (Fig. 2). A flexible loop region connecting both domains is comprised of residues 68–77 and 145–149. The essential PLP cofactor is linked covalently to Lys-56 forming a Schiff base, and the PLP site motifs 54(S*X*KIRG)59, 313(S*X*GN)316, and 185(GGGG)188 are conserved as found in other members of the $\beta$-family of PLP enzymes (29). A manganese ion is octahedrally coordinated by the acid groups of residues Glu-210 and Asp-216, the backbone carbonyl oxygen of Ala-214, and three water molecules. The side-chain amine group of Arg-135 and the carboxylic acid group of the malonate ligand form a salt bridge type ionic interaction in a compact active site. Arg-135 may perform a similar role to the "arginine finger" seen in the active site of G-proteins in stabilization of the reaction transition state to enhance the reaction rate (31, 32).

The crystal structure of the rat enzyme was determined in the ligand-free and malonate-bound form at 2.1- and 2.2-Å resolution, respectively (Fig. 2, *b* and *c*). For the malonate complex, one monomer (Monomer A) was well ordered, and all residues except for 1 and 324–333 were well defined, including a solvent-exposed loop region of the small domain (residues 69–73). The ordering of residues 69–73 in monomer A is favored by stabilizing crystal lattice contacts with helix 9 of the neighboring A monomer. Leu-72 has a water-mediated interaction with Lys-221, and Glu-73, Gly-74, and Lys-75 are involved in interactions with Lys-221, Leu-222, and Tyr-218 of the symmetry-related monomer A.

The second monomer (Monomer B) of the rat malonate complex was less well defined in the electron density with higher overall *B*-factors. In Monomer B residues 1–3 and 324–333 were disordered (consistent with Monomer A), furthermore, the loop residues 67–75 that were ordered in monomer A could not be resolved. The corresponding loop region was disordered in the malonate complex of human structure as well and constitutes a highly mobile region of mammalian SR. In the holo-form of rSR residues 3–323 were visible with the exception of small domain residues 128–137 and 144–150, which were disordered in both Monomers A and B. The rat holoenzyme and malonate complex of serine racemase have two molecules associated into a dimer. The dimer interface of rSR is conserved in the malonate complex of hSR via a 2-fold crystallographic axis and indicates a consistent dimeric form for mammalian serine racemase that is in agreement with other biophysical data reported herein. An analysis of the structural alignment of the human and rat monomers shows that they are well aligned with a $C_\alpha$ r.m.s.d. of 0.62 Å$^2$. However, when the human and rat dimers are aligned, using a single monomer for the superimposition, the average r.m.s.d. of the second monomer rises to 1.71 Å. Alignment of the uncomplexed rat dimer with the rat malonate complex increases the r.m.s.d. even further to 2.19 Å indicating greater conformational differences between the free and complexed structures. The human dimer has a buried monomer-monomer surface area of 840.6 Å$^2$, the rat complex 736.8 Å$^2$, and the rat uncomplexed dimer 827 Å$^2$. Although the role of crystal packing forces on the dimer inter-

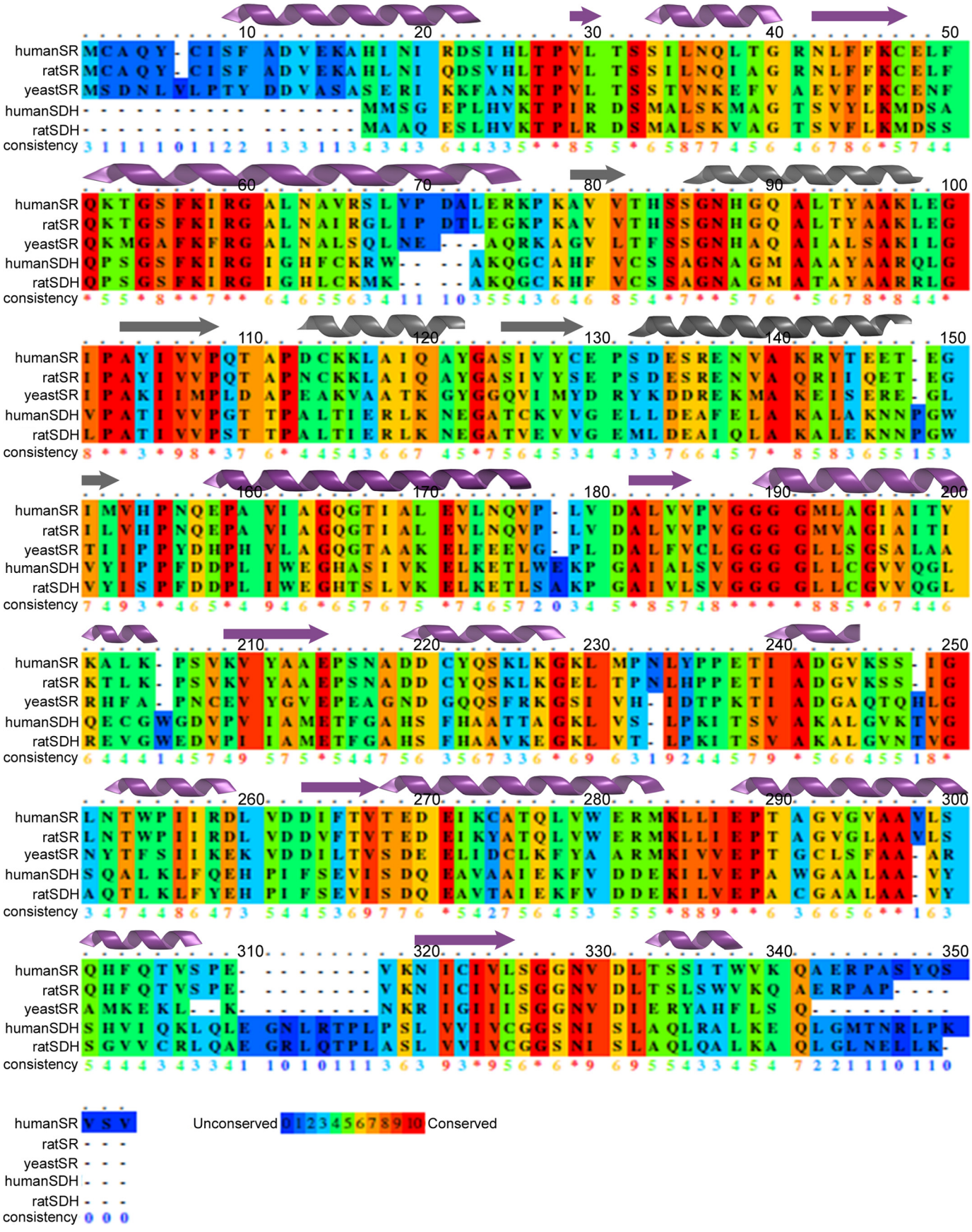


FIGURE 1. **Multiple-sequence alignment of human, rat, and yeast racemases with human and rat serine dehydratase.** Human SR and rat SR are 91% identical, and the sequence of human SR shares 23% identity with human SDH. There is ~90% structural similarity between SR and SDH. The small domain secondary structure of mammalian SR (residues 78–155) is in *gray*.

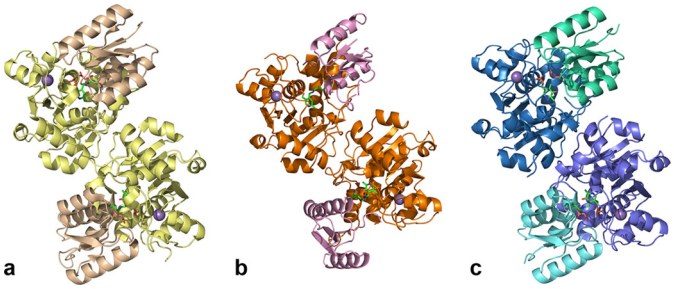


FIGURE 2. *a*, schematic representation of the rSR-malonate complex symmetric dimer with malonate (*orange*) and PLP (*green*) at the dimer interface. The large domain is colored *yellow*, and the small domain is *light brown*. *b*, rSR holoenzyme dimer. The large and small domains are colored *orange* and *pink*. *c*, schematic structure of human SR dimer. The small domains are displayed in *light blue*, and the catalytic domains are in *dark blue*. The human dimer is generated by a crystallographic axis of symmetry and is consistent with the rat dimer.

face cannot be discounted, the variation observed in the structures reported suggests a high degree of flexibility at the dimer interface.

## DISCUSSION

*Comparison of Mammalian and Yeast Crystal Structures*—Human and rat SR are 90% identical in sequence and are structurally almost indistinguishable. The malonate complex formed by either orthologue can be compared with the ligand-free rat structure with similar results. Using a monomer of malonate-bound human and holo rat enzymes for a structural alignment over all the residues shows that the large domains superimpose almost identically with an r.m.s.d. of 0.288 Å. There are, however, large differences in the small domain orientation as indicated by elevation of the r.m.s.d. to 0.711 Å with the small domains included. The small domain is shifted away from the PLP in the ligand-free structure with the exception of H4 (residues 85–98), which remains in the same position in both molecules with only a slight shift at the top of the helix (residue 98) when compared with the malonate complex (Fig. 3).

There is 40% sequence identity between the *S. pombe* SR sequence and the human and rat. A comparison of the *S. pombe* crystal structures (1V71 and 1WTC) with the human and rat structures reveals strong overall structural similarity. The yeast structure with and without ATP was determined by Goto and colleagues to 1.7 and 1.9 Å, respectively, both having accessible PLP sites. The large domains superimpose well with the mammalian structures with an r.m.s.d. of 1.30 Å, but differences are obvious in the orientation of the small domain as the r.m.s.d. increases to 1.76 Å for the whole structure (Fig. 3). In this region of the protein there is a distance of 4.5 Å between the ends of helix 6 (residues 131–147) in the yeast and the mammalian malonate-bound orthologs where the Arg-135 side chain is orientated in toward the PLP within the catalytic site. The small domain of the yeast is also rotated away from the PLP site with respect to the large domain exposing a channel into the PLP.

In the crystal structure of the rat malonate complex the loop residues (68–77) that constitute the flexible hinge region in the A monomer are ordered and adopt an extended loop conformation that may be typical of the orientation of these residues in mammalian SR enzymes. In the open yeast structure the loop (67–75) is ordered into an α-helix, and this is one of the areas of divergence from the mammalian SR. This protein region is less

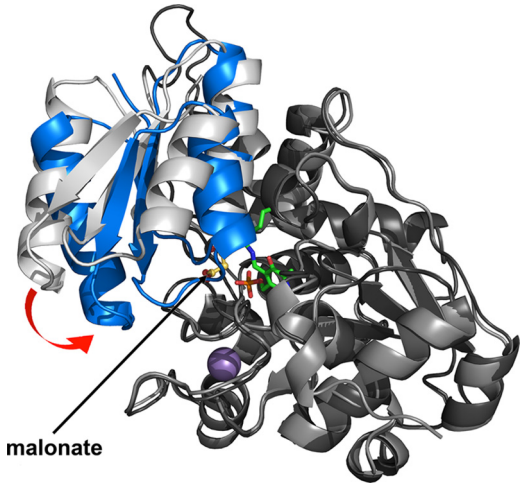


FIGURE 3. **Structural alignment of rat holo (*gray*) and complexed human (*blue*) serine racemase.** The small domain of each molecule has a different orientation with respect to the large domain (*gray*). *Curved arrows* at the base of H5 and H6 indicate the direction of movement from unbound (open) to ligand-bound (closed) conformation.

conserved, and the yeast has a deletion of three amino acids when compared with the mammalian sequence.

Comparison of the inhibitor-bound human structure with the rat holo and yeast structure indicate a closed conformation for the human complex and an open conformation for the yeast and rat holo-SR. There is also a large degree of flexibility and accommodation at the intradomain interface that allows the small domain to adopt different orientations in each of the crystal structures. The range of motion of the small domain may be larger, and is likely to be continuous and fluid rather than the three discrete poses captured, to date, by the crystal structures. This is suggested by one of our human holo structures where the small domain was fully disordered, highlighting the mobility in this region.[3] The motion of the domains in the context of the reaction mechanism will be discussed in the next section.

*Reaction Mechanism*—The SR-mediated reaction mechanisms are displayed in Fig. 4, according to the proposed scheme by Yoshimura and Goto (33, 34). For isomerization the L-serine Cα-hydrogen is replaced by the hydrogen from the hydroxyl group of Ser-82 of the human SR, which attacks the Cα from the opposite side to where the Cα-hydrogen was removed. The elimination reaction requires the removal of water with the hydroxyl group from Cβ of L-serine and hydrogen from the lysyl-$NH_3$ as leaving groups. After the water is removed, lysine replaces the aminoacrylate, which is then transformed to pyruvate.

Previous structural studies have provided information on the key features that allow the convergently evolved PLP enzymes to have similar reaction mechanisms. Comparisons of the SR and its closest homologue, SDH, which have structural similarity of >90%, reveal identical transition states with respect to their catalyzed reactions. The hSR crystal structure provides a rationale for its capability to perform two different reactions. Both enzymes can catalyze the elimination of water from serine, whereas only the SR can mediate the conversion of L-serine to its D-isomer and *vice versa*. The isomerization of L-serine is

[3] M. Smith, V. Mack, A. Ebneth, I. Moraes, B. Felicetti, M. Wood, D. Schonfeld, O. Mather, A. Cesura, and J. Barker, unpublished results.

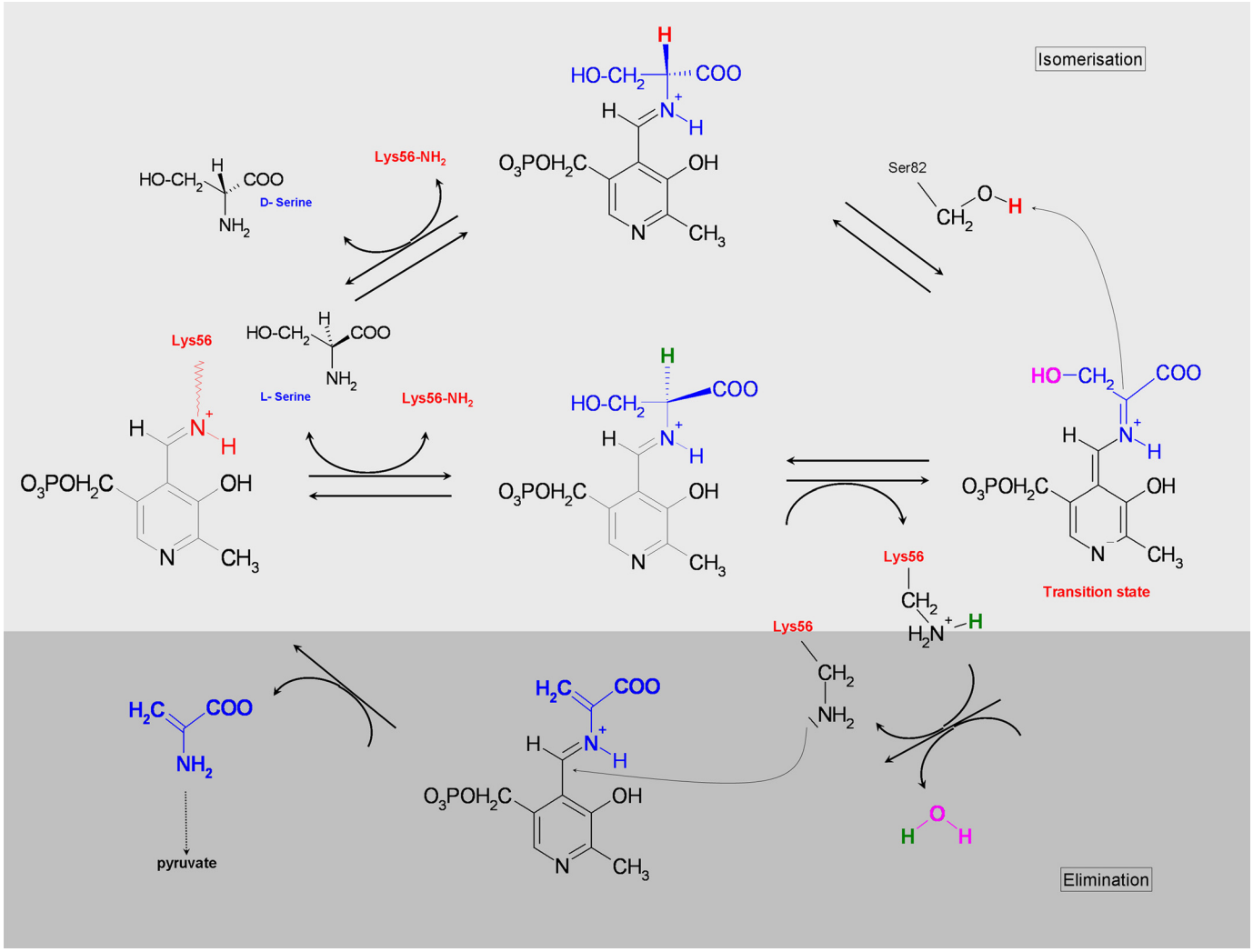


FIGURE 4. **The racemase and dehydratase reaction mechanism of serine racemase.** The racemase can attack the L-serine with either Ser-84 or Lys-56. The Ser-84 hydrogen from the hydroxyl side-chain attacks the C$\alpha$ from the opposite side to where the L-serine C$\alpha$-hydrogen was removed and racemization occurs resulting in D-serine. Or the lysyl-NH3-group and the hydroxyl-group from C$\beta$ of L-serine lose H and OH, respectively, to form water and follow the dehydratase reaction path. In the transition state a planar sp2-configuration of the L-serine C$\alpha$ is created by removal of the C$\alpha$-hydrogen at which point the racemase can proceed with either reaction.

dependent on the serine residue at position 84, which donates the proton to mediate this particular reaction. In contrast SDH, which has an alanine at this position, is devoid of racemase activity and can, therefore, also not use the D-isomer as substrate.

Mutagenesis studies reported by Yoshimura and Goto (33) showed the essential role of Ser-84 for the isomerization of serine and the consumption of D-serine. They found that a Ser-82 SR mutant from *D. discoideum* lost racemase and D-serine dehydratase activity but retained its capability to act as an L-serine dehydratase. This provides evidence for the crucial function of Ser-82 for racemization, which appears to be responsible for shuttling the transition state either into racemization of L-serine or allowing the D-serine to pass the transition state toward dehydratation (Fig. 4).

*Ligand-induced Shift of Small and Large Domains of the Racemase*—It is interesting to compare the new structures of mammalian serine racemase complexed with malonate to the yeast open structure and to the serine dehydratase bound to the inhibitor L-serine *O*-sulfate. We provide several lines of evidence suggesting that the small domain of the racemase, upon binding to the substrate or inhibitor, undergoes a major structural change placing Ser-84 into close proximity to the substrate and in an ideal orientation to donate the proton required for isomerization.

First, it can easily be seen that the catalytically active residue Ser-84 in the mammalian racemase is in close proximity to the C$\alpha$ of L-serine (2.6 Å) to allow the hydroxyl group to drive the transition state into racemization. The corresponding residue Ala-65 in the dehydratase is almost identically positioned although being catalytically inactive. The yeast racemase ortholog, free of substrate and inhibitor, shows the small domain helix (H6, residues 132–144) to be tilted away from the catalytic site by almost 4.5 Å as compared with the corresponding helices of the human (131–147) and rat complexed racemases (131–147). The small domain of the yeast structure is also differently orientated with respect to the corresponding helix of SDH (residues 113–126), which reflects the closed conformation of mammalian SR. The catalytically active Ser-82 in

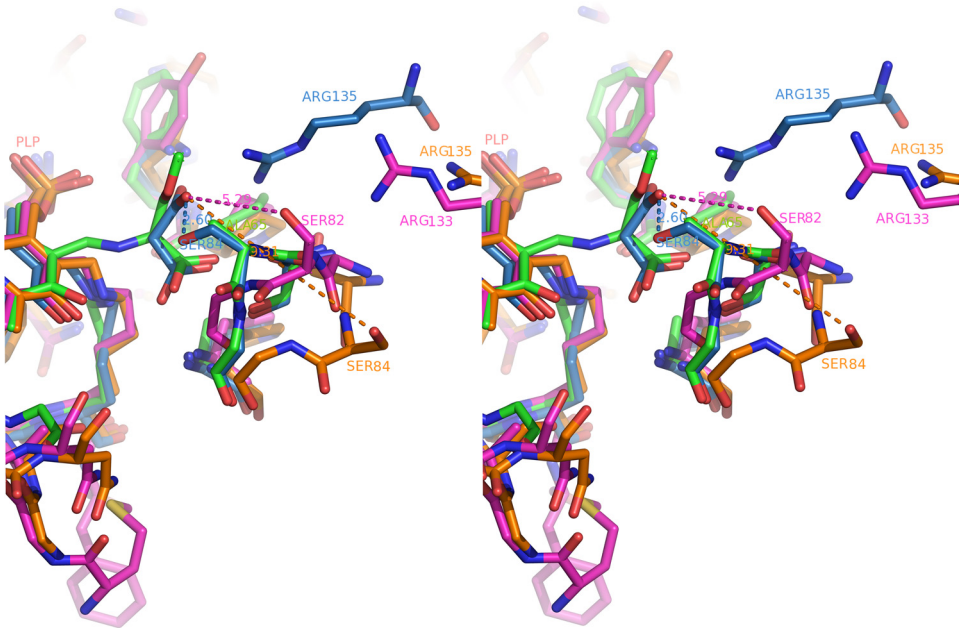


FIGURE 5. **Overlay of the PLP site of human serine racemase (*blue*), holo rat serine racemase (*orange*), yeast serine racemase (*magenta*), and rat serine dehydratase (*green*).** The catalytic serine in yeast SR and rat SDH is too far from the malonate or *O*-methyl serine (5.29 and 9.31 Å, respectively) for any reactions to occur in its open conformation. The human SR and rat SDH active sites overlay well both ligands in similar conformation. The catalytically inactive dehydratase Ala-65 is superbly aligned with the catalytic racemase Ser-84.

the yeast structure is shifted to a position where it cannot participate in the turnover of L-serine, because it is too distant to allow the hydroxyl group to donate the proton (5.29 Å). In addition, Ser-82 is tilted away by the helix displacement and, therefore, its hydroxyl group does not point to the catalytically active site (Fig. 5). The catalytic Ser-84 of the holo rat is positioned even further away from the ligand and represents an even greater opening between the large and small domains, into the active site than for the yeast structure.

Second, it is evident from the closed structures of the malonate-bound racemases that the access of L-serine to the catalytic site is hardly possible because of the very tight cleft between the large and the small domains. Hence, it appears likely that both domains need to move apart to create a gateway for the substrate and that binding of substrate or inhibitor triggers an induced shift of the small domain toward the catalytic site, which puts Ser-84 into the correct position toward the L-serine. This mechanism suggests that both subdomains are linked via a flexible hinge region.

Recent publications provide further support for the hypothesis that the small domain has to undergo an induced shift to allow the binding of the substrate. It has been shown that the racemase can be inhibited by binding to phosphatidylinositol (4,5)-bisphosphate, which is accomplished by several conserved lysine residues (33). Three of these residues (Lys-75, Lys-77, and Lys-96) shown to be involved in phosphatidylinositol (4,5)-bisphosphate-mediated inactivation of SR, reside in or close to the small domain, and two of those in direct vicinity of the catalytically active Ser-84 in the loop region (Lys-75 and Lys-77). It may be of interest that this loop is unique to mammalian racemases and absent in all other orthologs. Hence, it might be speculated that this region controls the activation of SR by allowing the substrate induced fit to occur only upon release of the enzyme from its membrane anchor phosphatidylinositol (4,5)-bisphosphate. Indeed, it has been shown that serine racemase seems to be kept in an inactivated state when associated to membranes and becomes activated only upon release into the cytosol. This process seems to be intimately linked to NMDAR activity, thus, providing feedback control to avoid excessive NMDAR activation (35). A similar small domain movement as described above has been suggested by Chen *et al.* to occur also in the PLP-dependent bacterial aspartate decarboxylase upon substrate binding (25). However, this hypothesis is based on the three-dimensional structure of the holoenzyme only and with no substrate-bound enzyme available. This may suggest a highly conserved reaction mechanism within this family of enzymes.

In summary the x-ray crystal structures reported here have confirmed that the domains of serine racemase are connected by a flexible linker and can adopt different orientations with respect to each other. The crystal structures correspond to biophysical data and confirm the dimeric state of the enzyme. Based on the motion of the domains observed between the unbound and ligand-bound structures we have redefined the domain boundaries of serine racemase in relation to the closely related type II PLP-dependent enzyme, SDH. The orthosteric inhibitor, malonate, adopts the binding pose of the cognate substrate, serine, in the active site of the closed structures. The racemization reaction is critically dependent on the proximity of the catalytic Ser-82 to the substrate as shown by the closed ligand-bound structures. The structures of SR we have reported represent starting points for rational drug design and suggest the possibility of modulating the enzymatic activity possibly by blocking the movement of the small domain.

*Acknowledgments—We thank Dr. Young-Hwa Song for supporting our crystallographic efforts and for technical input. We also thank Dr. John Kemp for his advice, discussion, and critical review of the manuscript.*

## REFERENCES

1. Johnson, J. W., and Ascher, P. (1987) *Nature* **325,** 529–531
2. Kleckner, N. W., and Dingledine, R. (1988) *Science* **241,** 835–837
3. Panatier, A., Theodosis, D., Mothet, J. P., Touquet, B., Pollegioni, L., Poulain, D. A., and Oliet, S. H. (2006) *Cell* **125,** 775–784
4. Matsui, T., Sekiguchi, M., Hashimoto, A., Tomita, U., Nishikawa, T., and Wada, K. (1995) *J. Neurochem.* **65,** 454–458
5. Schell, M. J., Brady, R. O., Jr., Molliver, M. E., and Snyder, S. H. (1997) *J. Neurosci.* **17,** 1604–1615
6. Mothet, J. P., Parent, A. T., Wolosker, H., Brady, R. O., Jr., Linden, D. J., Ferris, C. D., Rogawski, M. A., and Snyder, S. H. (2000) *Proc. Natl. Acad.*

*Sci. U.S.A.* **97,** 4926–4931
7. Yang, Y., Ge, W., Chen, Y., Zhang, Z., Shen, W., Wu, C., Poo, M., and Duan, S. (2003) *Proc. Natl. Acad. Sci. U.S.A.* **100,** 15194–15199
8. Wolosker, H., Sheth, K. N., Takahashi, M., Mothet, J. P., Brady, R. O., Jr., Ferris, C. D., and Snyder, S. H. (1999) *Proc. Natl. Acad. Sci. U.S.A.* **96,** 721–725
9. Basu, A. C., Tsai, G. E., Ma, C. L., Ehmsen, J. T., Mustafa, A. K., Han, L., Jiang, Z. I., Benneyworth, M. A., Froimowitz, M. P., Lange, N., Snyder, S. H., Bergeron, R., and Coyle, J. T. (2009) *Mol. Psychiatry* **14,** 719–727
10. Nagata, Y. (1992) *Experientia* **48,** 753–755
11. Inoue, R., Hashimoto, K., Harai, T., and Mori, H. (2008) *J. Neurosci.* **28,** 14486–14491
12. Chaffey, H., and Chazot, P. L. (2008) *Curr. Anaesthesia Crit. Care* **19,** 183–201
13. Brown, D. G., and Krupp, J. J. (2006) *Curr. Topics Med. Chem.* **6,** 649–650
14. Sheldrick, G. M. (2008) *Acta Crystallogr. Sect. A* **64,** 112–122
15. Abrahams, J. P., and Leslie, A. G. (1996) *Acta Crystallogr. D Biol. Crystallogr.* **52,** 30–42
16. Perrakis, A., Morris, R., and Lamzin, V. S. (1999) *Nat. Struct. Biol.* **6,** 458–463
17. Murshudov, G. N., Vagin, A. A., and Dodson, E. J. (1997) *Acta Crystallogr. D Biol. Crystallogr.* **53,** 240–255
18. Leslie, A. G. (1992) *Joint CCP4 + ESF-EAMCB Newsletter on Protein Crystallography*, No. 26
19. Collaborative Computational Project, No. 4 (1994) *Acta Crystallogr. D Biol. Crystallogr.* **50,** 760–763
20. Evans, P. R. (1997) *SCALA. Joint CCP4 ESF-EACBM Newsletter* **33,** 22–24
21. McCoy, A. J., Grosse-Kunstleve, R. W., Adams, P. D., Winn, M. D., Storoni, L. C., and Read, R. J. (2007) *J. Appl. Crystallogr.* **40,** 658–674
22. Pflugrath, J. W. (1999) *Acta Crystallogr. D Biol. Crystallogr.* **55,** 1718–1725
23. Emsley, P., and Cowtan, K. (2004) *Acta Crystallogr. D Biol. Crystallogr.* **60,** 2126–2132
24. DeLano, W. L. (2003) *PyMOL Reference Manual*, DeLano Scientific LLC, San Carlos, CA
25. Chen, H. J., Ko, T. P., Lee, C. Y., Wang, N. C., and Wang, A. H. (2009) *Structure* **17,** 517–529
26. Cook, S. P., Galve-Roperh, I., Martínez del Pozo, A., and Rodríguez-Crespo, I. (2002) *J. Biol. Chem.* **277,** 27782–27792
27. Hoffman, H. E., Jirásková, J., Ingr, M., Zvelebil, M., and Konvalinka, J. (2009) *Protein Expr. Purif.* **63,** 62–67
28. Strísovský, K., Jirásková, J., Mikulová, A., Rulísek, L., and Konvalinka, J., (2005) *Biochemistry* **44,** 13091–13100
29. Yamada, T., Komoto, J., Takata, Y., Ogawa, H., Pitot, H. C., and Takusagawa, F. (2003) *Biochemistry* **42,** 12854–12865
30. Sun, L., Bartlam, M., Liu, Y., Pang, H., and Rao, Z. (2005) *Protein Sci.* **14,** 791–798
31. Rittinger, K., Walker, P. A., Eccleston, J. F., Nurmahomed, K., Owen, D., Laue, E., Gamblin, S. J., and Smerdon, S. J. (1997) *Nature* **388,** 693–697
32. Scheffzek, K., Ahmadian, M. R., Kabsch, W., Wiesmüller, L., Lautwein, A., Schmitz, F., and Wittinghofer, A. (1997) *Science* **277,** 333–338
33. Yoshimura, T., and Goto, M. (2008) *FEBS J.* **275,** 3527–3537
34. Goto, M., Yamauchi, T., Kamiya, N., Miyahara, I., Yoshimura, T., Mihara, H., Kurihara, T. Hirotsu, K., and Esaki, N. (2009) *J. Biol. Chem.* **284,** 25944–25952
35. Balan, L., Foltyn, V. N., Zehl, M., Dumin, E., Dikopoltsev, E., Knoh, D., Ohno, Y., Kihara, A., Jensen, O. N., Radzishevsky, I. S., and Wolosker, H. (2009) *Proc. Natl. Acad. Sci. U.S.A.* **106,** 7589–7594


Protein Structure and Folding:

# The Structure of Mammalian Serine Racemase: EVIDENCE FOR CONFORMATIONAL CHANGES UPON INHIBITOR BINDING

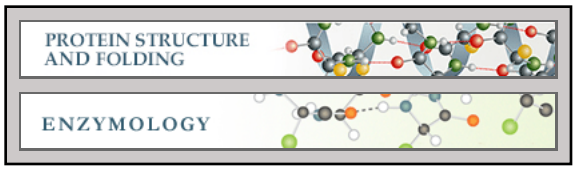


Myron A. Smith, Volker Mack, Andreas Ebneth, Isabel Moraes, Brunella Felicetti, Michael Wood, Dorian Schonfeld, Owen Mather, Andrea Cesura and John Barker

*J. Biol. Chem. 2010, 285:12873-12881.*
*doi: 10.1074/jbc.M109.050062 originally published online January 27, 2010*

---